

Ultra compact 45 GHz CMOS compatible Germanium waveguide photodiode with low dark current

Christopher T. DeRose,^{1,*} Douglas C. Trotter,¹ William A. Zortman,¹
Andrew L. Starbuck,¹ Moz Fisher,² Michael R. Watts,³
and Paul S. Davids¹

¹Sandia National Laboratory Applied Microphotonic Systems P.O. Box 5800, Albuquerque,
New Mexico 87185, USA

²IQE Silicon Compounds St. Mellons, Cardiff, CF3 0LW, UK

³Massachusetts Institute of Technology Research Laboratory of Electronics 77 Massachusetts
Avenue, Cambridge, Massachusetts 02139, USA

[*cderose@sandia.gov](mailto:cderose@sandia.gov)

Abstract: We present a compact $1.3 \times 4 \mu\text{m}^2$ Germanium waveguide photodiode, integrated in a CMOS compatible silicon photonics process flow. This photodiode has a best-in-class 3 dB cutoff frequency of 45 GHz, responsivity of 0.8 A/W and dark current of 3 nA. The low intrinsic capacitance of this device may enable the elimination of transimpedance amplifiers in future optical data communication receivers, creating ultra low power consumption optical communications.

© 2011 Optical Society of America

OCIS codes: (040.5160) Photodetectors; (060.4510) Optical communications; (040.6040 Silicon).

References and links

1. D. Ahn, C.-Y. Hong, J. Liu, W. Giziewicz, M. Beals, L. C. Kimerling, J. Chen, F. X. Kartner and J. Michel, "High performance, waveguide integrated Ge photodetectors" *Opt. Express* **15**, 3916–3921 (2007).
2. T. Yin, M. M. Morse, G. Sarid, Y. Chetrit, D. Rubin and M. J. Paniccia, "31 GHz Ge n-i-p waveguide photodetectors on Silicon-on-Insulator substrate" *Opt. Express* **15**, 13965–13971 (2007).
3. G. Masini, S. Sahni, G. Capellini, J. Witzens and C. Gunn, "High-Speed Near Infrared Optical Receivers Based on Ge Waveguide Photodetectors Integrated in a CMOS Process," *Advances in Optical Technologies* 196572 (5 pp.) (2008).
4. M. Oehme, J. WWerner, M. Kaschel, O. Kirfel and E. Kasper, "Germanium waveguide photodetectors integrated on silicon with MBE," *Thin Solid Films* **517**, 137–139 (2008).
5. L. Vivien, J. Osmond, J.-M. Fedeli, D. Marris-Morini, P. Crozat, J.-F. Damlencourt, E. Cassan, Y. Lecunff and S. Laval, "42 GHz p.i.n. Germanium photodetector integrated in a silicon-on-insulator waveguide," *Opt. Express* **1**, 6252–6257 (2009).
6. D. Feng, S. Liao, P. Dong, N.-N. Feng, H. Liang, D. Zheng, C.-C. Kung, J. Fong, R. Shafihah, J. Cunningham, A. V. Krishnamoorthy and M. Asghari, "High-speed Ge photodetector monolithically integrated with large cross-section silicon-on-insulator waveguide," *Appl. Phys. Lett.* **95**, 261105 (2009).
7. X. Zheng, F. Liu, D. Patil, H. Thacker, Y. Luo, T. Pinguet, A. Mekis, J. Yao, G. Li, J. Shi, K. Raj, J. Lexau, E. Alon, R. Ho, J. E. Cunningham and A. Krishnamoorthy, "A sub-picojoule-per-bit CMOS photonic receiver for densely integrated systems," *Opt. Express* **18**, 204–211 (2010).
8. M. S. Rasras, D. M. Gill, M. P. Earnshaw, C. R. Doerr, J. S. Weiner, C. A. Bolle and Y.-K. Chen, "CMOS Silicon Receiver Integrated With Ge Detector and Reconfigurable Optical Filter," *IEEE Photon. Technol. Lett.* **22**, 112–114 (2010).
9. J. Michel, J. Liu and L. C. Kimerling, "High-performance Ge-on-Si photodetectors," *Nature Photonics* **4**, 527–534 (2010).

10. S. Liao, N.-N. Feng, D. Feng, P. Dong, R. Shafihah, C.-C. Kung, H. Liang, W. Qian, Y. Liu, J. Fong, J. E. Cunningham, Y. Luo and M. Asghari, "36 GHz submicron silicon waveguide germanium photodetector," *Opt. Express* **19**, 10967–10972 (2011).
11. D. A. B. Miller, "Device Requirements for Optical Interconnects to Silicon Chips," *Proc. IEEE* **97**, 1167–1185 (2009).
12. M. R. Watts, D. C. Trotter, R. W. Young and A. L. Lentine, "Ultralow Power Silicon Microdisk Modulators and Switches," in *Proceedings of IEEE International Conference on Group IV Photonics* (IEEE, 2008) pp.4–6.
13. M. R. Watts, D. C. Trotter, R. W. Young and A. L. Lentine, "Maximally confined silicon microphotonic modulators and switches," in *Proceedings of LEOS* (IEEE, 2008) pp. 457–458.
14. M.R. Watts, D. C. Trotter, R. W. Young, A. L. Lentine and W. A. Zortman, "Limits to Silicon Modulator Bandwidth and Power Consumption," *Proc. SPIE* **7221**, 72210M-1–72210M-8 (2009).
15. M. R. Watts, W. A. Zortman, D. C. Trotter, G. N. Nielson, D. L. Luck and R. W. Young, "Adiabatic resonant microrings (ARMs) with directly integrated thermal microphotronics," in *2009 Conference on Lasers and Electro-Optics (CLEO)*, (Optical Society of America, 2009) paper CPDB10.
16. M. R. Watts, W. A. Zortman, D. C. Trotter, R. W. Young and A. L. Lentine, "Low-Voltage, Compact, Depletion-Mode, Silicon Mach-Zehnder Modulator," *IEEE J. Sel. Topics Quatum Electron.* **16**, 159–164 (2010).
17. W. A. Zortman, M. R. Watts, D. C. Trotter, R. W. Young and A. L. Lentine, "Low-Power High-Speed Silicon Microdisk Modulators," in *2010 Conference on Lasers and Electro-Optics (CLEO)*, (Optical Society of America, 2010) paper CThJ4.
18. C. T. DeRose, M. R. Watts, D. C. Trotter, D.L. Luck, G. N. Nielson and R. W. Young, "Silicon Microring Modulator with Integrated Heater and Temperature Sensor for Thermal Control," in *2010 Conference on Lasers and Electro-Optics (CLEO)*, (Optical Society of America, 2010) paper CThJ3.
19. W. A. Zortman, D. C. Trotter, A. L. Lentine, G. Robertson and M. R. Watts, "Monolithic Integration of Silicon Electronics and Photonics," in *2011 IEEE Winter Topicals (WTM)*, (IEEE, 2011) pp. 139–140.
20. C. T. DeRose, M. R. Watts, R. W. Young, D. C. Trotter, G. N. Nielson, W. A. Zortman and R. D. Kekatpure, "Low power and broadband 2x2 silicon thermo-optic switch," in *Optical Fiber Communication Conference* (Optical Society of America, 2011) paper OThM3.
21. J. Liu, D. D. Cannon, K. Wada, Y. Ishikawa, S. Jongthammanurak, D. T. Danielson, J. Michel and L. C. Kimerling, "Tensile strained Ge p-i-n photodetectors on Si platform for C and L band telecommunications," *Appl. Phys. Lett.* **87**, 011110 (2005).
22. M. Jutzi, M. Berroth, G. Wohl, M. Oehme and E. Kasper, "Ge-on-Si Vertical Incidence Photodiodes With 39-GHz Bandwidth," *IEEE Photon. Technol. Lett.* **17**, 1510–1512 (2005).
23. M. Morse, O. Dosunmu, G. Sarid and Y. Chetrit, "Performance of Ge-on-Si p-i-n Photodetectors for Standard Receiver Modules," *IEEE Photon. Technol. Lett.* **18**, 2442–2444 (2006).
24. M. Oehme, J. Werner, E. Kasper, M. Jutzi and M. Berroth, "High bandwidth Ge p-i-n photodetector integrated on Si," *Appl. Phys. Lett.* **89**, 071117 (2006).
25. H.-C. Luan, D. R. Lim, K. K. Lee, K. M. Chen, J. G. Sandland, K. Wada and L. C. Kimerling, "High-quality Ge epilayers on Si with low threading-dislocation densities," *Appl. Phys. Lett.* **75**, 2909–2911 (1999).
26. G. Masini, L. Colace, G. Assanto, H.-C. Luan and L. C. Kimerling, "High-Performance p-i-n Ge on Si Photodetectors for the Near Infrared: From Model to Demonstration," *IEEE Trans. Electron Devices* **48**, 1092–1096 (2001).
27. L. Colace, P. Ferrara, G. Assanto, F. Fulgoni and L. Nash, "Low Dark-Current Germanium-on-Silicon Near-Infrared Detectors," *IEEE Photon. Technol. Lett.* **19**, 1813–1815 (2007).
28. L. Colace, and G. Assanto, "Germanium on Silicon for Near-Infrared Light Sensing," *IEEE Photon. J.* **1**, 69–79 (2009).
29. M. A. Omar and L. Reggiani, "Drift Velocity and Diffusivity of Hot Carriers in Germanium: Model Calculations," *Solid State Electron.* **30**, 1351–1354 (1987).

1. Introduction

The success of the silicon electronics industry is primarily due to its high yield, low cost, high volume manufacturing and the doubling of transistor density every two to three years . Although the density of transistors continues to grow exponentially, the bandwidth of electrical IO does not. The poor scaling of data communication may lead to a performance bottleneck in future generation CPUs. Furthermore, in order to continually improve CPU performance manufacturers are now using chip multi-processor technology, placing increased demand on data communication bandwidth. Complementary metal oxide semiconductor (CMOS) compatible silicon photonics has been identified as the most likely candidate for future generation data communication interconnects both in the back plane of high performance computing nodes and

within an optically interconnected multi-core processor.

A key component for CMOS compatible silicon photonics is a photodiode capable of detecting light in the near infrared. Recently there have been a number of demonstrations of vertical waveguide Ge p-i-n on silicon photodiodes with device areas ranging from ($800\text{--}60\ \mu\text{m}^2$) [1–10]. In order to create a “receiverless” system (eliminating the need for a transimpedance amplifier (TIA)), $\sim 1\ \text{fF}$ capacitance photodiodes will be required [11]. Hence, compact Ge photodiodes with best-in-class performance metrics are highly desirable. Here we present an ultra compact ($5.2\ \mu\text{m}^2$) Germanium waveguide photodiode which has been integrated into Sandia National Laboratories CMOS compatible silicon photonics process [12–20]. Due to its ultra low intrinsic capacitance of only $1.2\ \text{fF}$, this compact photodiode may enable direct driving of a transistor gate, eliminating the need for a TIA and drastically reducing power consumption in CMOS compatible data communication links. Due to its low capacitance and small device area this photodiode has low dark current ($3\ \text{nA}$) and is capable of operating at data rates in excess of $40\ \text{Gbps}$. Furthermore, we show through a design of experiments reducing the dimensions of vertical n-i-p photodiodes leads to the most sensitive and highest bandwidth device.

2. Diode fabrication

The typical approach to vertically illuminated Ge detectors on Si has been to utilize a top-down approach where blanket epitaxy is grown over the entire wafer area and then features are defined by lithography and etching [21–24]. The optoelectronic devices fabricated with such an approach are dominated by recombination at dislocations introduced to relieve the misfit strain. We have taken a bottom-up approach, where Ge epitaxy grows only in exposed windows (selective area growth) of a field oxide. This approach lends itself to dislocation reduction because the dislocations that form are much closer to the window edge and can terminate on this surface [25].

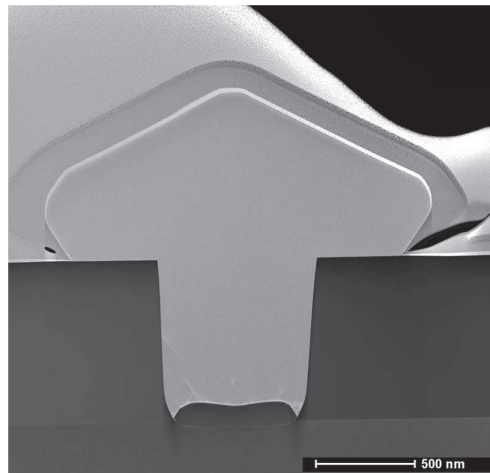


Fig. 1. TEM cross-section of selective area epitaxially grown Ge structure showing overgrowth before CMP and low threading dislocation defect density.

Using selective area growth in an oxide trench on top of a Si pedestal, Germanium waveguide photodiodes have been integrated into Sandia’s CMOS compatible silicon photonics process flow as follows: High Density Plasma (HDP) oxides are used for initial cladding of the silicon and nitride waveguides to an approximate $1\ \mu\text{m}$ thickness, after which patterning of

oxide windows for Ge growth is completed. The selective Ge epitaxy consists of a low temperature buffer layer grown at 400 °C and in-situ doped with boron to a carrier concentration of $\sim 1E18 \text{ cm}^{-3}$ followed by a growth at 600 °C and pressure of 10 mTorr to fill and overgrow the oxide windows, allowing for chemical-mechanical polish (CMP) planarization. The final Germanium thickness was targeted at 0.6 μm . A high resolution transmission electron micrograph (TEM) cross-section of the overgrown oxide trenches is shown in Fig. 1.

Phosphorous was implanted and activated to a concentration of $1E19 \text{ cm}^{-3}$ to form the n-type layer and top contact of the diode, deposition of a capping oxide to completed the formation of the vertical n-i-p diode structure. Rapid thermal anneal (RTA) activation of the implants is done at 630 °C for 30 seconds. The n-i-p Ge diode's anode is contacted with parallel contacts in the Si pedestal which was implanted with Boron and activated to a concentration of $1E19 \text{ cm}^{-3}$ prior to growth. Ohmic electrical contact to the active silicon and germanium regions was accomplished with a two step contact process: First Ti/TiN sputter depositions were used to form titanium/silicon as well as titanium/germanium contacts to all n+ and p+ regions in both materials and second, vias were filled with tungsten. CMP planarization completed the contact formation. Metal electrical interconnects were formed by deposition and patterning of a 1 μm Ti/TiN/AlCu/TiN stack. The final optical cladding is a plasma enhanced chemical vapor deposition (PECVD) oxide, which was deposited to a thickness of 2.5 μm prior to bond pad opening for electrical connection. A device schematic and scanning electron micrograph (SEM) cross section of a completed Ge photodiode are shown in Fig. 2(a) and (b) respectively.

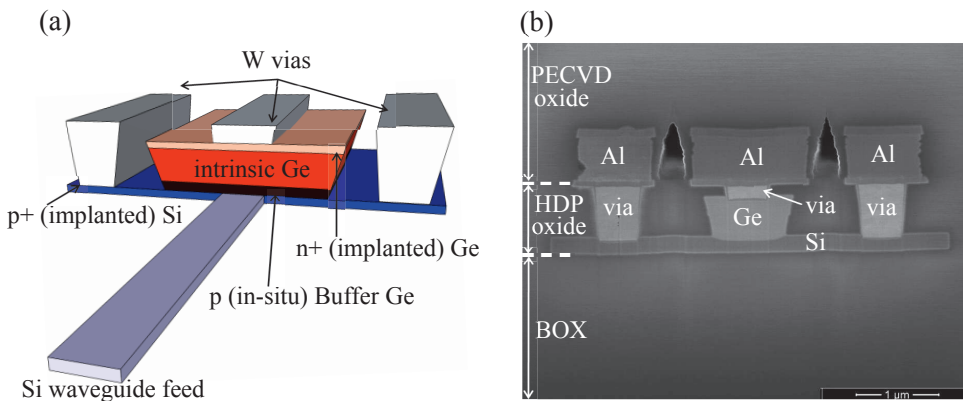


Fig. 2. (a) Schematic of Germanium waveguide n-i-p photodiode. (b) SEM cross-section of final selective area epitaxially grown Ge photodiode with final electrical contacts.

3. Experimental results

Ge photodiodes with widths ranging from 1.3 to 5.3 μm and lengths ranging from 4 to 64 μm were fabricated. The fabricated photodiodes were characterized for dark current (i_{dark}), responsivity (\mathcal{R}), 3 dB bandwidth (f_{3dB}) and noise equivalent power (NEP), with results summarized in Table 1.

The dark current was measured as a function of reverse bias, with the lowest measured dark current densities of $\sim 40 \text{ mA/cm}^2$ at 1 V reverse bias. From these measurements we find a linear increase in dark current density with width of the photodiode. This indicates an increase in threading dislocation density for wider photodiodes, likely due to greater defect annihilation at the side of the oxide trench for the narrower devices. It was previously reported that the threading dislocation density can be decreased by more than an order of magnitude by adding

Table 1. Summary of the measured characteristics of integrated Ge photodiodes for different width (W) x length (L) geometries. * estimated from $C = \varepsilon \cdot A/d$, ** measured at 1 V reverse bias, † measured at 1.5 μm wavelength, ‡ measured at a wavelength of 1.5 μm for the TM polarization, § measured at 1.53 μm wavelength with 1 V reverse bias and a DC photocurrent of 300 μA .

W (μm)	L (μm)	C^* (fF)	i_{dark}^{**} (nA)	NEP^\dagger (W/Hz $^{1/2}$)	$\mathcal{R}^{\ddagger\dagger}(A/W)$	f_{3dB}^{\ddagger} (GHz)
1.3	4	1.2	3	3.8E-14	0.80	45
1.3	8	2.4	5	4.8E-14	0.83	41
1.3	16	4.8	9	6.2E-14	0.85	43
1.3	32	9.6	31	1.2E-13	0.84	41
1.3	64	19.2	70	1.7E-13	0.86	32
2.3	4	2.2	20	9.0E-14	0.88	39
2.3	8	4.4	29	1.1E-13	0.91	42
2.3	16	8.8	43	1.3E-13	0.89	36
2.3	32	17.6	161	2.5E-13	0.90	34
2.3	64	35.2	254	3.0E-13	0.93	25
5.3	4	5.0	165	2.3E-13	0.97	33
5.3	8	10.0	156	2.1E-13	1.05	26
5.3	16	20.0	350	3.1E-13	1.05	28
5.3	32	40.0	407	3.5E-13	1.01	21
5.3	64	80.0	1510	6.6E-13	1.04	14

a post growth anneal step to the process [25–28]. Thus it is likely that with further process development, an added anneal step will reduce dark current densities to $\sim 1 \text{ mA/cm}^2$. Fig. 3(a) shows the measured dark current density at 1 V reverse bias as a function of diode width where each point represents an average of 11 measurements and Fig. 3(b) shows a typical set of IV curves for a photodiode 1.3 μm wide with lengths ranging from 4–64 μm .

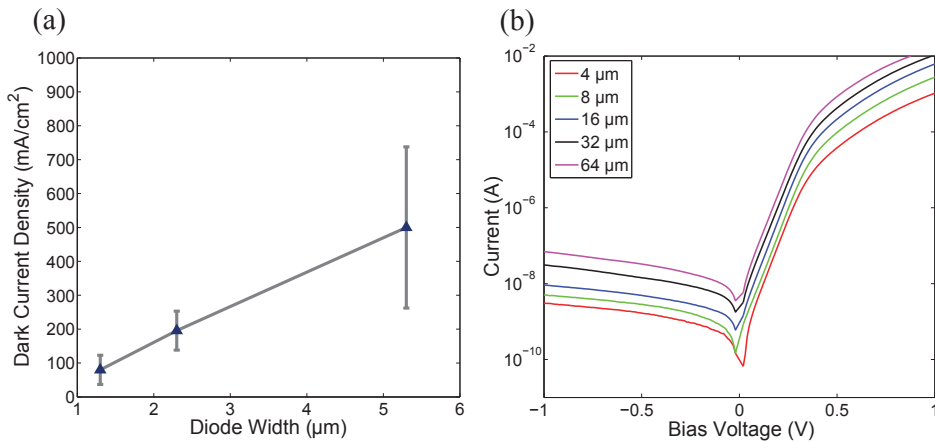


Fig. 3. (a) Measured linear trend between dark current density at 1 V reverse bias and photodiode width. Each point is the average of 11 separate measurements. (b) Typical set of IV curves for photodiode 1.3 μm wide for various lengths.

The fiber to waveguide coupling losses and waveguide propagation losses up to the photodiode were calibrated out of the responsivity measurements. We find that the maximum respon-

sivity of the n-i-p photodiodes has a slight dependence on diode width, due to the increased coupling efficiency of the silicon waveguide mode to the modes of the wider diodes. As expected, there is also an increase in diode responsivity with device length as seen in Fig. 4(a). Interestingly, since the increase in diode responsivity due to both larger width and length is accompanied by an increase in dark current which increases shot noise more rapidly than responsivity, the larger diodes have a higher NEP and are therefore less sensitive detectors. This result can be seen in Fig. 4(b) and leads us to the conclusion that the smaller the photodiode the more sensitive the detector and the lower the detector intrinsic capacitance.

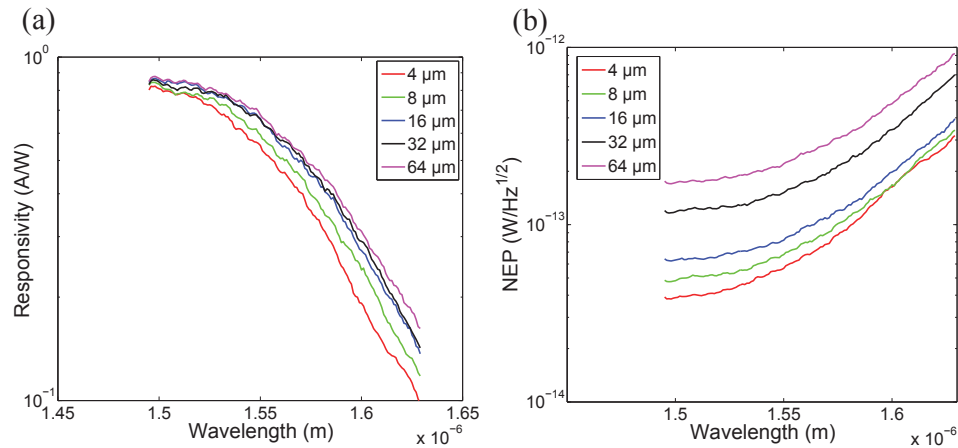


Fig. 4. (a) Measured responsivity for 1.3 μm wide Ge waveguide photodiodes with various lengths, measured with -10 dBm of TM polarized light (b) NEP as a function of wavelength for the same 1.3 μm wide Ge photodiodes, measured for -10 dBm of TM polarized light.

A large built in electric field is highly desirable for CMOS compatible photodiodes. Large internal electric fields enable operation at the carrier velocity saturation bandwidth with low applied reverse bias voltages. Maintaining low voltage operation is critical for detector compatibility with current and future CMOS voltage levels and allows for low power dissipation and low dark currents. In Germanium, field strengths on the order of 1E4 V/cm are required to reach carrier velocity saturation in holes [29]. If we use

$$V_{bi} = \frac{k_B T}{q} \log \left(\frac{N_A N_D}{n_i^2} \right) \quad (1)$$

where k_B is the Boltzmann constant, T is temperature in kelvin, q is the electron charge, N_A is the density of acceptors in the p region, N_D is the density of donors in the n region and n_i is the intrinsic carrier concentration, to estimate the built in potential (V_{bi}). A value of \sim 1E4 V/cm for the built in field is calculated. This result suggests that high speed, carrier velocity saturation bandwidth operation for moderate to large optical powers can be obtained with low applied reverse bias voltages in this device. Evidence of a strong built in field can be seen in Fig. 5(a) where no roll off of the photocurrent is observed at 0V bias and an open circuit voltage of 0.4 V is measured.

The 3 dB bandwidth was measured using the heterodyne note of two ultra-stable, narrow line-width Agilent 81600B lasers. The lasers were combined with a 50/50 beam splitter with the wavelength one laser was held constant at 1530 nm and the other was stepped in 100 MHz increments up to 50 GHz, beginning at 1530 nm. The power of each laser was kept equal and such that the total DC photocurrent was 300 μA . The RF power extracted from the photodiode

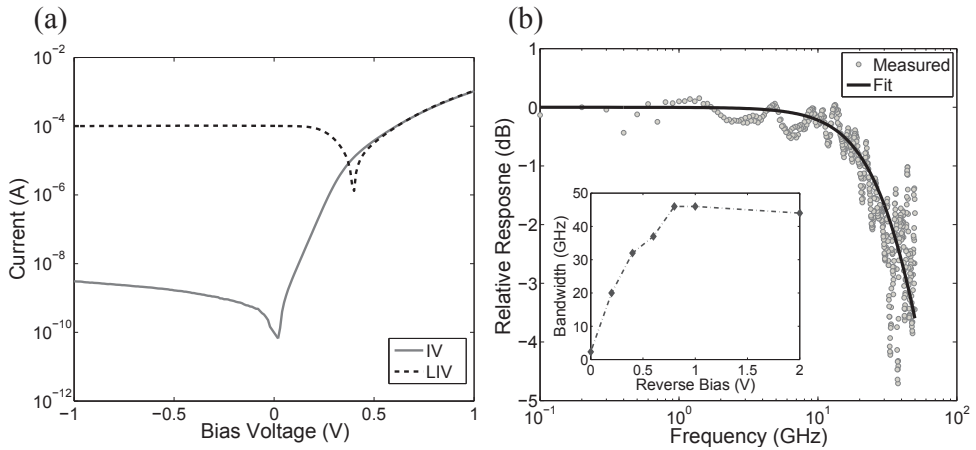


Fig. 5. (a) Dark current-voltage (IV) and Illuminated ($\lambda = 1.53 \mu\text{m}$) current-voltage (LIV) characteristics of a $1.3 \times 4 \mu\text{m}^2$ Ge photodiode (b) Bandwidth of $1.3 \times 4 \mu\text{m}^2$ Ge photodiode at 2 V reverse bias, measured using an optical heterodyne technique showing a 3-dB roll off frequency of 45 GHz. Inset shows saturation of bandwidth at 0.8 V reverse bias for a photocurrent of $300 \mu\text{A}$.

from GSG probes was then measured on an Agilent E4419B RF power meter with a 50 GHz power meter head. The measurement was calibrated to the device under test (DUT) using an Agilent E8364B 50 GHz vector network analyzer. The results of the measurement were fit to a single pole frequency response, which was used to determine the device 3 dB bandwidth. Fig. 5(b) illustrates a typical measured data and curve fit. We found that the largest measured bandwidth was 45 GHz, for the $1.3 \times 4 \mu\text{m}^2$ detector with larger area diodes having slightly lower bandwidths. This result is better than the best bandwidth previously reported for this class of detector [5]. Furthermore, we found that for a relatively large photocurrent of $300 \mu\text{A}$ the bandwidth of the diodes saturated below 1V reverse bias (see Fig. 5(b) inset), another strong indication of a large internal electric field. Although the bandwidth roles off at 0V bias due to carrier screening effects for the relatively large photocurrent of 0.3 mA , we found that with a photo-current of $30 \mu\text{A}$ the photodiode had a bandwidth of 37 GHz at 0V bias, giving further confirmation that low voltage operation is possible. This result demonstrates that these devices can be operated at high speed using current and future CMOS voltage levels.

4. Conclusions

We have fabricated and characterized integrated Ge waveguide photodiodes in a process flow which is fully compatible with Sandia's CMOS electronics and active silicon photonics platforms. We find that reducing photodiode dimensions to $1.3 \times 4 \mu\text{m}^2$ leads to the most sensitive, lowest capacitance and highest bandwidth integrated photodiode with a dark current of only 3 nA, and a responsivity of 0.8 A/W . To the best of the authors knowledge, this result demonstrates a device which has best-in-class bandwidth performance and the lowest intrinsic device capacitance ($\sim 1 \text{ fF}$) thus far reported in the literature. This ultra compact integrated photodiode may enable "receiverless" optical links with ultra low power dissipation in future data communication systems.

Acknowledgments

Funding for this work was provided by Sandia's Laboratory Directed Research and Development (LDRD) program and the Department of Defense. Sandia is a multiprogram laboratory operated by Sandia Corporation, a Lockheed Martin Company, for the United States Department of Energy's National Nuclear Security Administration under contract DE-AC04-94AL85000.